Energy & Environmental Science

Cite this: *Energy Environ. Sci.*, 2011, **4**, 5008

www.rsc.org/ees

PAPER

Enzymatic biofuel cells designed for direct power generation from biofluids in living organisms†

Takeo Miyake,[ab] Keigo Haneda,[a] Nobuhiro Nagai,[c] Yohei Yatagawa,[a] Hideyuki Onami,[c] Syuhei Yoshino,[a] Toshiaki Abe[c] and Matsuhiko Nishizawa*[ab]

Received 22nd July 2011, Accepted 16th September 2011
DOI: 10.1039/c1ee02200h

Enzymatic biofuel cells have attracted much attention for their potential to directly use biochemical energy sources in living organisms such as animals, fruits, *etc.* However, generally natural organisms have a skin, and the oxygen concentration in the organisms is lower than that of biofuels like sugars. Here, we fabricated a novel miniature assembly that consists of a needle bioanode for accessing biofuels in organisms through their skins and a gas-diffusion biocathode for utilizing the abundant oxygen in air. The performance of the biocathode was fourfold improved by optimizing its hydrophobicity. The assembled device with four needle anodes for fructose oxidation was inserted into a raw grape, producing a maximum power of 26.5 μW (115 μW cm^{-2}) at 0.34 V. A light-emitting diode (LED) with the cell served as a self-powered indicator of the sugar level in the grape. Power generation from blood sugar was also investigated by inserting a needle anode for glucose oxidation into a blood vessel in a rabbit ear. Prior coating of the tip of the needle anode with an anti-biofouling agent was effective to stabilize the output power.

Introduction

An enzymatic biofuel cell is a type of fuel cell where enzymatic catalysts are used to convert the chemical energy of biological fuels into electricity, instead of the metallic catalysts commonly used in fuel cells.[1–9] The high reaction selectivity of enzymes results in unique advantages, including the possibility of power generation from biofluids such as juices and bloods without purification. For example, Dong *et al.* have reported the energy-harvesting from natural fruit juices.[10,11] Furthermore, Mano *et al.* have demonstrated direct power generation in a grape berry using a glucose oxidase (GOD)-modified fine anode and a bilirubin oxidase (BOD)-modified fine cathode; both are inserted into a peeled grape.[12]

In the present investigation, we attempt to develop a miniature insertion device for energy harvesting from living organisms without any pretreatments. Such a device entails the following considerations. (1) Natural organisms are generally covered by a skin. (2) Oxygen in the organism is limited to a lower concentration than sugars.[13,14] (3) Biofluids contain reaction inhibitors for cathodic enzymes, such as ascorbic acid[15] and urate.[16,17] (4) Blood will form a clot on the surface of inserts. In order to address these considerations, our present device has been designed as shown in Fig. 1, which consists of a needle

[a]*Department of Bioengineering and Robotics, Tohoku University, 6-6-1 Aramaki Aoba, Aoba-ku, Sendai, 980-8579, Japan. E-mail: nishizawa@biomems.mech.tohoku.ac.jp; Tel: +81 22 795 7003*
[b]*Core Research for Evolutional Science and Technology (CREST), Japan Science and Technology Agency, Tokyo, 102-0075, Japan*
[c]*Division of Clinical Cell Therapy, United Centers for Advanced Research and Translational Medicine (ART), Graduate School of Medicine, Tohoku University, 2-1 Seiryo-machi, Aoba-ku, Sendai, 980-8575, Japan*
† Electronic supplementary information (ESI) available: See DOI: 10.1039/c1ee02200h

Broader context

Power generation from the carbohydrates and alcohols produced by living systems is an attractive potential green energy technology, and has motivated for decades the development of enzymatic biofuel cells that can directly generate electricity without purification of the biofluids. In this study, we fabricated miniature biofuel cells that consist of a needle bioanode for accessing biofuels in organisms and a gas-diffusion biocathode for utilizing the abundant oxygen present in air. By inserting the needle into a grape, a light-emitting diode was powered to blink with a frequency corresponding to the fructose concentration in the berry. Also, power generation from blood sugar was demonstrated by inserting the needle into a rabbit vein. Such needle-based biofuel cells can be expected to serve in the future as the power unit of biodevices for environmental or healthcare monitoring.

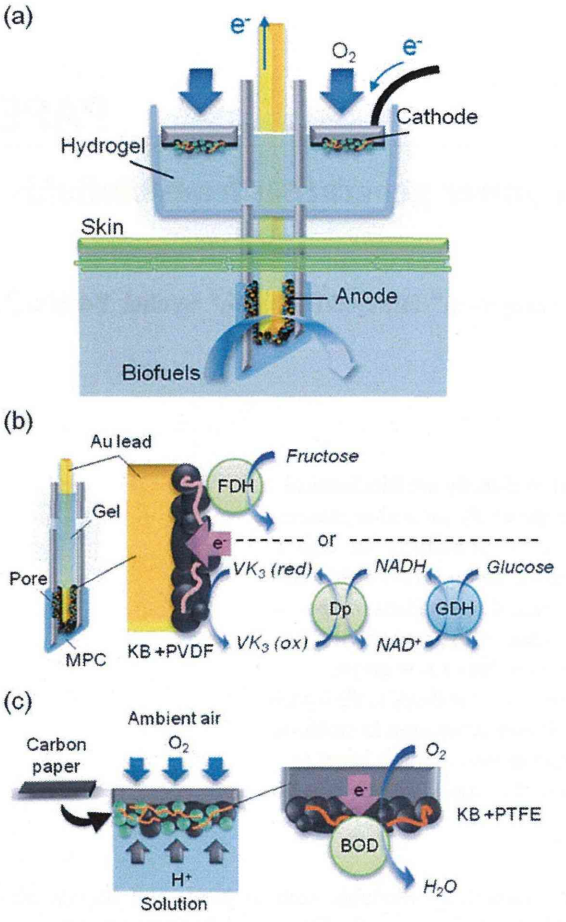

Fig. 1 (a) Schematic structure of a biofuel cell designed to utilize biochemical energy in living organisms. (b) Schemes of oxidation of fructose and glucose at the enzymatic needle anodes. (c) Schemes of O_2 reduction at the enzymatic gas-diffusion cathode.

bioanode for oxidation of fructose or glucose inside living organisms (Fig. 1b), and a carbon paper-based gas-diffusion biocathode for reduction of the abundant oxygen in the ambient air (Fig. 1c). This anode and cathode are assembled using an ion-conducting agarose hydrogel as the inner matrix. This novel structural design allows insertion into the organisms even through tough skins, and protects the cathode from reaction inhibitors present in the biofluids.

Experimental section

Fabrication of needle anodes

Both ends of an eppendorf plastic needle or one end of an SUS syringe (TERUMO, 25G) was cut as shown in Fig. S1†. The SUS needle was insulated by electrodeposition of anodic electrophoretic paint (ELECOAT AE-X, SHIMIZU, applied voltage: 10 V, deposition time: 3 min). After inserting gold wire into these needles, a 1% solution of agarose containing buffer salts (80 °C) is injected into the internal needle space and cooled in air. Since the hydrogel-filled needle blocks the subsequent injection of enzyme solutions, 1 mm diameter holes were drilled in the sidewall of the needles to reduce the inner pressure. As we explain in the Results and discussion section, the holes act also as effective windows for fuel supply.

The anode for fructose oxidation was prepared using a plastic needle and fructose dehydrogenase (FDH, EC 1.1.99.11, 160 U) from *Gluconobacter*. 2 μl of a solution containing ketjenblack (KB)/poly(vinylidene fluoride) (PVDF) (3 : 1, 10 mg ml^{-1}) was coated on the gold wires (*ca.* 0.057 cm^2 geometric surface area). After drying in air, the electrode was modified with a 3 mg ml^{-1} FDH solution, followed by drying in air.

An SUS needle was used for the anode for glucose oxidation with glucose dehydrogenase (GDH, EC 1.1.1.47, 250 U mg^{-1}) from *microorganism*, diaphorase (Dp, EC 1.6.99, 1000 U mg^{-1}) from *Clostridium*, Poly-L-Lysine-modified vitamin K_3 (PLL-VK_3) and nicotinamide adenine dinucleotide (PLL-NAD^+) according to the protocol previously described.[19–22] 4 μl PLL-VK_3 solution (4.83 mM) was mixed with a 3 μl Dp solution (14 mg ml^{-1}), 1 μl poly(ethylene glycol) diglycidyl ether (PEGDE, 10 mg ml^{-1}) solution and 3 μl KB solution (20 mg ml^{-1}). A 2.5 μl aliquot of the mixed solution was put on a gold wire (*ca.* 0.0032 cm^2 geometric surface area) and dried in air. The surface of a PLL-VK_3/Dp/KB electrode was coated with 2.4 μl of a solution containing a 40 mg ml^{-1} GDH solution, a 10 mg ml^{-1} PLL solution and a 50 mg ml^{-1} PLL-NAD^+.

Preparation of gas-diffusion cathodes

A solution containing KB/poly(tetrafluoroethylene) (PTFE) (1 : 1, 8 mg ml^{-1}) was put on a 0.2 mm thick Toray carbon paper (CP) and dried in air. A 4 mm diameter hole was previously punched at the center of the CP. The surface of the KB-modified CP electrode was modified with a 5 mg ml^{-1} solution of bilirubin oxidase (BOD, EC 1.3.3.5, 2.5 U mg^{-1}, from *Myrothecium*). After drying in air, the electrode was further coated with a mixed KB solution to make the surface hydrophobic. This enzyme-modified electrode was mounted on a chamber made from PDMS, which was filled with 1% agarose hydrogel containing buffer salts. The geometric surface area of the CP electrode was 0.67 cm^2 (the device for a grape) or 0.19 cm^2 (the device for a rabbit).

Electrochemical measurements

The anode and the cathode of the cell were connected through an analog-type variable resistor (range: from 2 MΩ to 28 Ω). The cell voltage and electrode potentials were measured against a homemade Ag|AgCl (saturated KCl) reference electrode by an electrochemical analyzer combined with LabVIEW (program: LabVIEW software, hardware for voltage detection: NI USB-6221) at given values of the resistance. The current and the power were derived from the detected cell voltage and the resistance.

The grape used is RED GLOBE (GROS COLMAN). *In vivo* measurements in the rabbits have been carried out in accordance with the guidelines of Tohoku University Environmental & Safety Committee (no. 22EgA-4). The rabbits were anesthetized with ketamine hydrochloride (35 mg kg^{-1}) and xylazine hydrochloride (5 mg kg^{-1}), awaking from anesthesia for 1 hour, by which time we would measure the cell voltage by inserting the anode of the cell into the ear veins of the rabbits.

Results and discussion

Performance of gas-diffusion biocathodes

Fig. 2a shows cyclic voltammograms of the gas-diffusion cathode at 10 mV s^{-1}. The carbon paper-based biocathodes were put on an oxygenic pH 7.0 buffer solution so as to contact the solution by the BOD-modified face (thin solid plot). The reduction current density reaches −0.5 mA cm^{-2} at 0 V, a value of which is twice that of a biocathode that was entirely immersed in the solution (broken plot). Such superior performance of a gas-diffusion cathode originates in the efficient supply of oxygen from the ambient air through the carbon paper.[23–26] The oxygen solubility in water is limited to ~0.3 mM and its diffusion coefficient is also small (2×10^{-5} cm^2 s^{-1}). In contrast, these values in air are orders of magnitude larger, *ca.* 10 mM and 2×10^{-1} cm^2 s^{-1}. The performance of an O_2-diffusion biocathode can be further improved by modifying the three-phase interface, consisting of the current collecting solid phase (enzyme-modified electrode), the electrolyte solution liquid phase, and the gas phase for oxygen supply.[16,27] For example, an additional coating of hydrophobic KB onto the BOD-modified face of the biocathode was effective in controlling excess penetration of liquid (Fig. 2b), which led to a fourfold performance up to *ca.* −2 mA cm^{-2} at 0 V (bold plot in Fig. 2a). This improved cathode will contribute to the miniaturization of the biofuel cell assembly as described later. Because the BOD enzyme shows activity over a wide pH range (pH 4–7), cathode performance of the same quality was observed even under acidic pH 5.0 conditions, as shown in Fig. S2†. Therefore, the present O_2-diffusion BOD cathode is applicable to experiments both of a grape with pH 5.0 gel and of a rabbit vein with pH 7.0 gel.

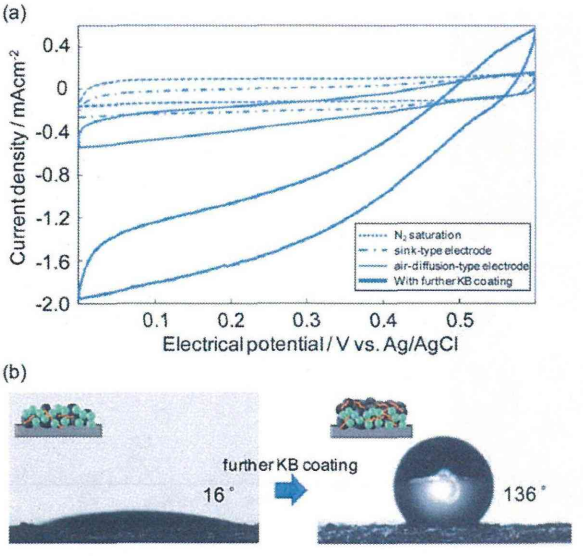

Fig. 2 (a) Cyclic voltammograms of O_2 reduction at BOD/KB (sink- and diffusion-type) and KB/BOD/KB (diffusion-type) electrodes at 10 mV s^{-1}. The control experiment in N_2-satuirated solution is also shown. (b) Photographs of water droplets placed on BOD/KB (contact angle = 16°) and KB/BOD/KB surfaces (contact angle = 136°).

Power generation from raw grapes

A biofuel cell device for fruits was constructed using the O_2-diffusion BOD cathode and the needle bioanode modified with FDH for fructose oxidation. These electrodes were mounted in a PDMS chamber filled with agarose hydrogel prepared with 750 mM McIlvaine buffer solution (pH 5.0). The device was inserted into a grape as shown in Fig. 3a, and at first the performance of the needle anode was evaluated using an externally inserted Ag/AgCl reference electrode (Fig. 3b). The needle anode without the side pore shows an oxidation current density of 0.35 mA cm^{-2} (current: 20.1 μA, geometric electrode area: 0.057 cm^2) at 0.6 V by oxidation of fructose that penetrated though the needle aperture. By opening the side pores, the anodic performance in a grape was enhanced up to 1.53 mA cm^{-2} (current: 87.6 μA) at 0.6 V.

Fig. 3c shows the cell performance using a raw grape at room temperature. The upper panel shows the cell voltage, the anode potential and the cathode potential as functions of the cell current, while the lower panel shows the cell power. The device generated 6.3 μW of electrical power (111 μW cm^{-1-2}) with a cell current of 25 μA at 0.25 V (0.23 V anodic potential and 0.48 V cathodic potential *vs.* Ag/AgCl). The cell performance was strongly dependent on the concentration of the buffer in the agarose gel. For example, the device using 30 mM buffered gel produced only 2.2 μW. Importantly, the total performance could be amplified by connecting an array of needle anodes in parallel; the device with the array of four needle anodes (Fig. S3†) had a fourfold output power, *ca.* 26.5 μW (Fig. 3d).

The raw grape contains not only fructose but also glucose at a similar concentration.[28,29] However, the GDH-based needle anode modified for glucose oxidation did not work well in the grape (Fig. S4†) because the activity of GDH is lowered in acidic conditions.[19–22]

As the final experiment using grapes, we demonstrate the possibility of monitoring sugar levels in the fruit. A FDH-based needle biofuel cell was combined with an LED device consisting of a charge pump IC, a 1 μF ceramic capacitor and a red LED. As we reported previously,[30] the blink interval of the LED is inversely proportional to the power of the biofuel cell, which is roughly proportional to the concentration of the biofuel. In practice, the LED blinks at a higher frequency with an increase in the fructose concentration (Fig. 3e), and the concentration of fructose within the grape was estimated to be roughly 20–40 mM. In fact, the power curve in the 35 mM fructose experimental solution was almost identical with that in the grape, as shown in Fig. S5†.

Power generation from a rabbit ear vein

Power generation from blood requires biocompatibility in order to prevent the formation of a blood clot on the electrode surface. To make the electrode biocompatible, a coating with 2-methacryloyloxyethyl phosphorylcholine (MPC)-polymer[31] is effective. In fact, as shown in Fig. 4a, an MPC-treated substrate resisted blood clotting even after immersion in blood for 2 hours. Fig. 4b shows cyclic voltammograms of the MPC-coated or uncoated GDH/PLL-NAD^+/Dp/PLL-VK_3 needle anodes in PBS solution containing 10 mM glucose. Both reached to current density of *ca.* 1.5 mA cm^{-2} (current: 5.0 μA, geometric electrode

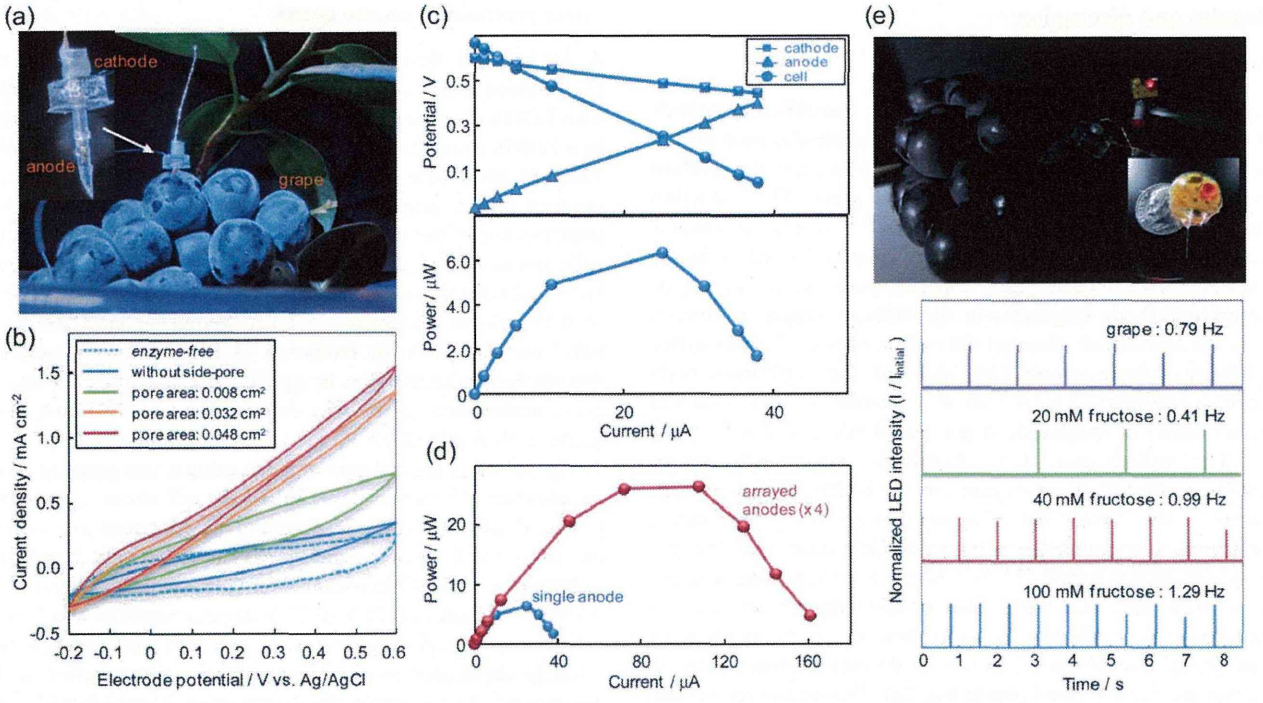

Fig. 3 (a) Photograph of the assembled biofuel cell inserted into a grape. (b) Cyclic voltammograms of FDH-modified needle anodes at 10 mV s^{-1} in a raw grape. Side pores were drilled in the wall of the needle (pore area: 0.008, 0.032 and 0.048 cm^2). (c) (upper panel) Polarization curve of the biofuel cell in the grape at room temperature. The cell voltage (●), the cathode potential *vs.* Ag/AgCl (■) and the anode potential *vs.* Ag/AgCl (▲) are plotted as function of the current density. (lower panel) Variation of the power with the cell current. (d) Power output of the biofuel cell using single anode and arrayed anodes (×4). (e) Monitoring of sugar level in a raw grape with a self-powered fructose-sensing devices. The device consists of the biofuel cell and an LED system, whose blink interval is correlated with the fructose concentration.

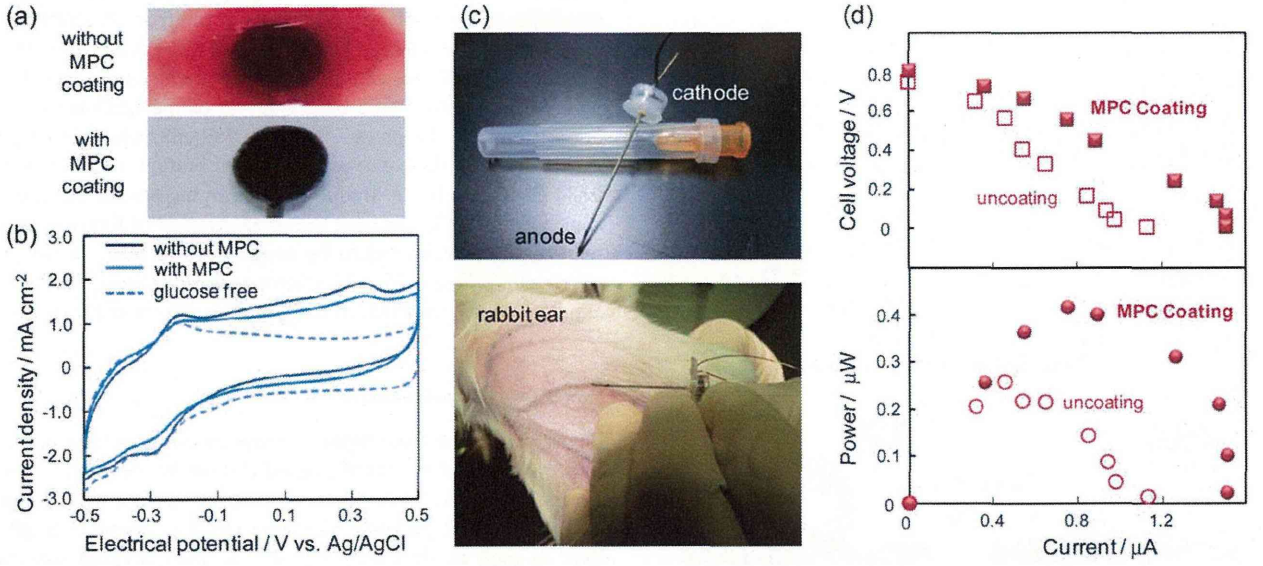

Fig. 4 (a) Photographs of electrode substrates with (and without) a MPC-coating, taken after soaking in withdrawn blood for 2 hours. (b) Cyclic voltammograms of bare and MPC-coated needle bioanodes at 10 mV s^{-1} in phosphate buffer containing 10 mM glucose. The control experiment (glucose-free) is also shown. The current density was estimated from the geometric area of the anode, 0.0032 cm^2. (c) Photographs of the assembled biofuel cell for power generation from a rabbit vein. (d) Performance of the biofuel cells using a needle anode, with and without MPC-coating, taken by inserting the needle anodes into a rabbit vein.

area: 0.0032 cm^2) at 0.5 V with a CV shape corresponding to glucose oxidation at GDH/PLL-NAD^+/Dp/PLL-VK_3 electrode.[19–21] These results indicate that the MPC coating serves as a bioinert layer without significant disturbance for the glucose transport to the enzyme electrodes inside the needle.

By assembling this needle anode with the O_2-diffusion BOD cathode, the fuel cell performance was evaluated by inserting it into a vein of a rabbit ear (Fig. 4c). Fig. 4d shows the typical current–voltage and current–power curves obtained by changing the external resistance (10 kΩ–2 MΩ). The open-circuit voltage of the cell was 0.81 V, which is similar to the difference between the potentials at which glucose oxidation and oxygen reduction start to occur in cyclic voltammograms (0.55 V in Fig. 2a and −0.30 V in Fig. 4b, respectively). The performance of the anode is reflected in the maximum cell current, 1.50 μA (466 μA cm^{-2}). The power for this cell reached 0.42 μW at 0.56 V, while the device without a MPC coating showed ~40% loss in power. Since the MPC coating has no significant effect on the electrode processes (Fig. 4b), the lowered performance is probably due to the formation of blood clots. In fact, after the insertion experiment, the formation of some biofilms was observed only on the needle anodes without the MPC coating. Probably, the blood clots interfere with the transport of glucose into the needle, and may also have effects on the cell resistance and kinetics.

Conclusions

We assembled a biofuel cell with a needle anode and gas-diffusion cathode, as a practical form of cell for direct power generation from natural organisms with skins. The results presented here include techniques to improve the performance of the devices. (1) A gas-diffusion cathode treated to be hydrophobic showed higher activity. (2) Incorporating side pores into the needles effectively enhanced the supply of biofluids to the inner anodes. (3) Modification of the needle tip with MPC polymer was required to obtain comparatively stable power from bloods. We also demonstrated that an array of needle anodes led to an increase in the output power (Fig. 3d). In the near future, a finer array of microscopic needle anodes will be fabricated by advanced micro-/nano-techniques for realizing a minimally invasive patchable biofuel cell system.

Acknowledgements

The authors thank Dr Yasuo Iwaki of the Biochemical Department, TOYOBO for the donation of enzymes. This work was partly supported by the Noguchi Institute.

References

1 I. Willner, E. Katz, *Bioelectronics*, Wiley-VCH, Weinheim, 2005.
2 G. T. R. Palmore, H. Bertschy, S. H. Bergens and G. M. Whitesides, *J. Electroanal. Chem.*, 1998, **443**, 155.
3 I. Willner, Y. M. Yan, B. Willner and R. T. Vered, *Fuel Cells*, 2009, **1**, 7.
4 M. J. Moehlenbrock and S. D. Minteer, *Chem. Soc. Rev.*, 2008, **37**, 1188.
5 W. Gellett, M. Kesmez, J. Schumacher, N. Akers and S. D. Minteer, *Electroanalysis*, 2010, **7-8**, 727.
6 A. Heller and B. Feldman, *Chem. Rev.*, 2008, **108**, 2482.
7 S. C. Barton, J. Gallaway and P. Atanassov, *Chem. Rev.*, 2004, **104**, 4867.
8 J. A. Cracknell, K. A. Vincent and F. A. Armstrong, *Chem. Rev.*, 2008, **108**, 2461.
9 J. Wang, *Talanta*, 2008, **75**, 636.
10 Y. Liu and S. Dong, *Biosens. Bioelectron.*, 2007, **23**, 593.
11 D. Wen, X. Xu and S. Dong, *Energy Environ. Sci.*, 2011, **4**, 1358.
12 N. Mano, F. Mao and A. Heller, *J. Am. Chem. Soc.*, 2003, **125**, 6588.
13 N. Mano, H. H. Kim, Y. Zhang and A. Heller, *J. Am. Chem. Soc.*, 2002, **124**, 6480.
14 S. Shleev, G. Shumakovich, O. Morozova and A. Yaropolov, *Fuel Cells*, 2010, **4**, 726.
15 X. Li, L. Zhang, L. Su, T. Ohsaka and L. Mao, *Fuel Cells*, 2009, **1**, 85.
16 C. Kang, H. Shin, Y. Zhang and A. Heller, *Bioelectrochemistry*, 2004, **65**, 82.
17 C. Kang, H. Shin and A. Heller, *Bioelectrochemistry*, 2006, **68**, 22.
18 P. Rowinski, C. Kang, H. Shin and A. Heller, *Anal. Chem.*, 2007, **79**, 269.
19 F. Sato, M. Togo, M. K. Islam, T. Matsue, J. Kosuge, N. Fukasaku, S. Kurosawa and M. Nishizawa, *Electrochem. Commun.*, 2005, **7**, 643.
20 M. Togo, A. Takamura, T. Asai, H. Kaji and M. Nishizawa, *Electrochim. Acta*, 2007, **52**, 4669.
21 M. Togo, A. Takamura, T. Asai, H. Kaji and M. Nishizawa, *J. Power Sources*, 2008, **178**, 53.
22 T. Miyake, M. Oike, S. Yoshino, Y. Yatagawa, K. Haneda and M. Nishizawa, *Lab Chip*, 2010, **10**, 2574.
23 G. Gupta, C. Lau, V. Rajendran, F. Colon, B. Branch, D. Ivnitski and P. Atanassov, *Electrochem. Commun.*, 2011, **4**, 247.
24 X. Wu, F. Zhao, J. R. Varcoe, A. E. Thumser, C. A. Rossa and R. C. T. Slade, *Biosens. Bioelectron.*, 2009, **24**, 326.
25 A. Habrioux, G. Merle, K. Servat, K. B. Kokoh, C. Innocent, M. Cretin and S. Tingry, *J. Electroanal. Chem.*, 2008, **579**, 97.
26 G. Gupta, C. Lau, B. Branch, V. Rajendran, D. Ivnitski and P. Atanassov, *Electrochim. Acta*, 2011, DOI: 10.1016/j.electacta.2011.01.089.
27 R. Kontani, S. Tsujimura and K. Kano, *Bioelectrochemistry*, 2009, **76**, 10.
28 W. M. Kliewer, *Am. J. Enol. Vitic.*, 1967, **18**, 33.
29 J. K. Palmer and W. B. Brandes, *J. Agric. Food Chem.*, 1974, **22**, 709.
30 T. Miyake, S. Yoshino, T. Yamada, K. Hata and M. Nishizawa, *J. Am. Chem. Soc.*, 2011, **133**, 5129.
31 K. Ishihara, T. Ueda and N. Nakabayashi, *Polym. J.*, 1990, **22**, 355.

Journal of Controlled Release 151 (2011) 65–73

Contents lists available at ScienceDirect

Journal of Controlled Release

journal homepage: www.elsevier.com/locate/jconrel

NANOMEDICINE

Suppression of phagocytic cells in retinal disorders using amphiphilic poly (γ-glutamic acid) nanoparticles containing dexamethasone

Morin Ryu [a], Toru Nakazawa [a,*], Takami Akagi [b,c], Tatsuhide Tanaka [d], Ryou Watanabe [a], Masayuki Yasuda [a], Noriko Himori [a], Kazuichi Maruyama [e], Toshihide Yamashita [e], Toshiaki Abe [f], Mitsuru Akashi [b,c], Kohji Nishida [a,g]

[a] Department of Ophthalmology, Tohoku Graduate University School of Medicine, 1-1 Seiryo, Aoba, Sendai, Miyagi 980-8574, Japan
[b] Department of Applied Chemistry, Graduate School of Engineering, Osaka University, 2-1 Yamadaoka, Suita, Osaka 565-0871, Japan
[c] Japan Science and Technology Agency (JST), Core Research for Evolutional Science and Technology (CREST), Tokyo, Japan
[d] Department of Molecular Neuroscience, Graduate School of Medicine, Osaka University, 2-2 Yamadaoka, Suita, Osaka 565-0871, Japan
[e] Department of Ophthalmology, Kyoto Prefectural University of Medicine, 465 Kajiicho, Hirokojiagaru Kawaramachi-dori, Kamigyo-ku, Kyoto 602-084, Japan
[f] Division of Clinical Cell Therapy, Center for Advanced Medical Research and Development, United Centers for Advanced Research and Translational Medicine, Tohoku University Graduate School of Medicine, 2-1 Seiryo, Aoba, Sendai, Miyagi 980-8575, Japan
[g] Department of Ophthalmology, Osaka University School of Medicine, 2-2 Yamadaoka, Suita, Osaka 565-0871, Japan

ARTICLE INFO

Article history:
Received 16 August 2010
Accepted 26 November 2010
Available online 3 December 2010

Keywords:
Drug delivery
Nanoparticles
Neuroprotection
Cytokines
Monocyte recruitment
Microglia

ABSTRACT

To investigate the potential of nanoparticles (NPs) composed of poly(γ-glutamic acid) conjugated with L-phenylalanine (γ-PGA-Phe NPs) for the treatment of retinal diseases, γ-PGA-Phe NPs (200 nm) were tested with macrophages and microglia *in vitro* or by intravitreal administration into normal or pathological rat eyes. The anti-inflammatory effects of the NPs containing dexamethasone (DEX-NPs) were examined using qRT-PCR *in vitro* by counting activated microglia and Fluorogold-labeled retinal ganglion cells in the retinas under excitotoxicity or by counting TUNEL (+) photoreceptors in the detached retinas. The NPs were taken up efficiently by cultured macrophages or microglia. At day 7, 60–80% of the diffuse signal remained in the cytoplasm of these cells. In normal rat eyes, the NPs did not accumulate in the retinas and no inflammatory cells were recruited. Conversely, under pathological conditions, the NPs were localized in activated CD11b-positive cells in the retina. DEX-NPs suppressed the expression of TNFα and MCP-1 in cultured macrophages or microglia, the activation of microglia, the loss of retinal ganglion cells (RGCs) in excitotoxic retinas, and the number of TUNEL (+) photoreceptors in detached retinas. These data suggest that γ-PGA-Phe NPs can be a powerful tool for suppressing inflammatory cells in pathological conditions in the retina.

1. Introduction

Various delivery systems have the potential to deliver drugs over extended periods of time to specific cells without systemic complications [1–3]. Previously, drug-encapsulating polymeric microparticles (1–1000 μm) or nanoparticles (NPs: 10–1000 nm) were used for clinical applications to achieve sustained drug delivery, where the rate drug release depends on the rate of polymer degradation. Those polymers include polylactide (PLA) [4], poly(lactide-*co*-glycolid) (PLGA) [5–7], acrylic polymers, copolymers, hyaluronic acid derivatives, and alginates. Among the available biodegradable polymers, PLA [4] and PLGA are the most widely used, with degradation rates ranging from months to years [5–7] depending on the composition and molecular weight of the substance being released. However, major problems associated with PLA and PLGA polymers include the low encapsulation efficiency of highly water-soluble proteins and the instability during formulation, storage, and lyophilization of the NPs. Instability of the proteins also occurs during polymer degradation due to the accumulation of acidic monomers and the consequent generation of a low pH inside the biodegradable NPs.

Another important facet of drug delivery is the route of administration or carrier device. Prior studies have investigated eye drops or systemic administration with very small NPs (less than 20 nm) [8], subconjunctival administration [4], trans-scleral drug delivery with a trans-scleral depot containing the drugs [9], scleral implants [10], transcorneal or trans-scleral iontophoresis [11,12] and aerosol administration during surgery for vitrectomy [13]. These local application techniques helped to minimize systemic complications and provided higher concentrations of the drugs in the posterior portion of the eyes.

In this study, we used poly(γ-glutamic acid) (γ-PGA) as the backbone of a biodegradable hydrophilic polymer and L-phenylalanine (Phe) as the hydrophobic side chain. γ-PGA is composed of naturally occurring D- and L-glutamic acid, γ-linked together through amide bonds [14–16]. The γ-PGA-*graft*-Phe copolymers can form NPs due to their amphiphilic properties [5]. Their ability to form NPs is attributed to the hydrophobic interactions between the Phe groups attached to

* Corresponding author. Tohoku Graduate University School of Medicine, Department of Ophthalmology, 1-1 Seiryo, Aoba, Sendai, Miyagi 980-8574, Japan. Tel.: +81 22 717 7294; fax: +81 22 717 7298.
E-mail address: ntoru@oph.med.tohoku.ac.jp (T. Nakazawa).

0168-3659/$ – see front matter © 2010 Elsevier B.V. All rights reserved.
doi:10.1016/j.jconrel.2010.11.029

the γ-PGA backbone resulting in the increased stability of the hydrophobic cores in the NPs. NPs consisting of γ-PGA-*graft*-Phe (γ-PGA-Phe NPs) have several important advantages as cytoplasmic delivery carriers including resistance to proteases, such as cathepsin [14], which accumulate in dendritic cells (DCs) and phagocytic cells such as macrophages. Our group [17–20] and others [21] have previously demonstrated that these antigen-loaded NPs represent a possible vaccine candidate for immune therapy. Moreover, γ-PGA-Phe NPs have been tested in several clinical applications including T cell tolerance of pollen antigen [21], vaccination for Japanese encephalitis [17], cancer treatment [18], and human immunodeficiency virus type 1 gp120 [19,20]. Hence, γ-PGA-Phe NPs have the potential for multiple clinical applications in the near future. However, the dynamics of NPs in the eye remains unclear.

In various pathological conditions, monocytes are recruited to the retina through the increased expression of cytokines and chemokines in a damaged area; in addition, resident microglia are also activated, then proliferate and migrate [22,23]. Physiologically, one of the major roles of phagocytic cells is to clean up the debris of dying cells [24]. In various pathological conditions, we have found that macrophages/microglia have a neurodestructive effect on damaged neurons via secreting cytokines or initiating oxidative stress [22,25–27]. Thus, the suppression of macrophages/microglia could be an important strategy for providing neuroprotection in various retinal disorders. In this study, we used γ-PGA-Phe NPs containing Texas Red-labeled ovalbumin (TR-OVA) to explore the dynamics of NPs in the eye. Next, we characterized the effects of γ-PGA-Phe NPs in cultured macrophages and microglia and then investigated the potential for using γ-PGA-Phe NPs containing dexamethasone (DEX-NPs) for *in vivo* immunosuppressive treatment of macrophages and microglia in various pathological conditions in the retinal.

2. Materials and methods

2.1. Animals

In total, 129 Sprague–Dawley (SD) rats (120 male and 9 female, weighing 250–300 g; Japan SLC, Hamamatsu, Japan) were used. For *in vivo* studies, we used 18 male rats (6 for each dosage of the NPs) to study normal conditions, 24 male rats to study the dynamics of NPs under pathological conditions (excitotoxicity and retinal detachment), 16 male rats to study DEX-NP treatment in a retinal detachment model, and 32 male rats to count surviving RGCs after DEX-NP treatment in the excitotoxic model. For *in vitro* experiments, 21 male rats were used for a macrophage culture and 90 rat pups (postnatal day 1 delivered from 9 female SD rats) for primary culture of microglia; another 9 male rats were used for a retina mixed culture. The surgical procedures were performed under deep anesthesia with intramuscular administration of a mixture of ketamine (100 mg/kg) and xylazine (9 mg/kg) or intraperitoneal injections of sodium pentobarbital (45 mg/kg, Vortech Pharmaceuticals). The rats were euthanized with an intraperitoneal injection of a lethal dose of pentobarbital (Fatal-Plus solution; 390 mg/ml).

All animals were maintained and handled in accordance with the ARVO Statement for the use of animals in Ophthalmic and Vision Research and the guidelines from the declaration of Helsinki and the Guiding Principles in the Care and Use of Animals. All experimental procedures described in the present study were approved by the Ethics Committee for Animal Experiments at Tohoku University Graduate School of Medicine. Animals were treated according to the National Institutes of Health guidelines for the care and use of laboratory animals.

2.2. Materials

γ-PGA ($M_w = 3.8 \times 10^5$, D-Glu/L-Glu = 60/40) was kindly donated by the Meiji Seika Co., Ltd. (Tokyo, Japan). L-phenylalanine ethyl ester (Phe) and dexamethasone (DEX) were purchased from Sigma (St. Louis, MO). 1-Ethyl-3-(3-dimethylaminopropyl) carbodiimide, dimethylsulfoxide (DMSO) and sodium hydrogen carbonate ($NaHCO_3$) were purchased from Wako Pure Chemical Industries (Osaka, Japan). 5-(Aminoacetamido) fluorescein and Texas Red-labeled OVA (TR-OVA) were purchased from Molecular Probes (Eugene, OR).

2.3. Preparation of γ-PGA-Phe NPs

γ-PGA-*graft*-L-phenylalanine (γ-PGA-Phe) was prepared by the conjugation of the L-phenylalanine ethyl ester (Phe) as previously described [14,15]. Briefly, γ-PGA (4.7 unit mmol) was hydrophobically modified by Phe (4.7 mmol) in the presence of 1-Ethyl-3- (3-dimethylaminopropyl) carbodiimide (4.7 mmol) in 50 mM $NaHCO_3$ (100 ml). The purified γ-PGA-Phe was characterized by ^1H NMR to determine the degree of Phe grafting. In this study, γ-PGA-Phe with 53% of Phe grafting was used. To analyze the intracellular distribution of the NPs, fluorescein-labeled γ-PGA-Phe (F-γ-PGA-Phe) was also synthesized using the same method in the presence of 5-(aminoacetamido) fluorescein (23.5 μmol). The amount of incorporated fluorescein was measured by spectrofluorometry. NPs composed of γ-PGA-Phe were prepared by a precipitation method. γ-PGA-Phe or F-γ-PGA-Phe (10 mg/ml) was dissolved in DMSO and this solution was added to saline at the same volume to yield a translucent solution. The resulting solution was then centrifuged at 14,000 × *g* for 15 min, rinsed repeatedly, and resuspended in phosphate-buffered saline (PBS) at a concentration of 20 mg/ml.

2.4. Preparation of TR-OVA-encapsulated NPs (TR-OVA-NPs)

To prepare the TR-OVA-encapsulated NPs, γ-PGA-Phe (10 mg/ml in DMSO) was added to the same volume of 2 mg/ml TR-OVA to yield a translucent solution. The resulting solution was centrifuged at 14,000 × *g* for 15 min and repeatedly rinsed to remove the organic solvent and free TR-OVA. Approximately 90% of the initial γ-PGA-Phe copolymer was recovered as NPs. The residual DMSO in the NP solution (20 mg/ml) was removed to below 1 ppm by the purification process. TR-OVA-encapsulated NPs (TR-OVA-NPs) were added to a volume of 4% sodium dodecyl sulfate (SDS) to dissolve the NPs, and the TR-OVA concentration in the TR-OVA-NP solution was measured by the Lowry method, as previously described [28,29]. From the estimated TR-OVA and NP concentrations in the sample solution, TR-OVA-NPs with a TR-OVA loading of 100 μg per milligram NP was prepared. The entrapment efficiency of TR-OVA into the NPs was calculated using the following formula: (amount of encapsulated TR-OVA / initial feeding amount of TR-OVA) × 100. The TR-OVA entrapment efficiency reached approximately 50%.

2.5. Preparation of dexamethasone-adsorbed NPs (DEX-NPs)

To prepare the DEX-NPs, γ-PGA-Phe NPs or F-γ-PGA-Phe NPs (F-NPs) (5 mg/ml in PBS) were mixed with DEX (1 mg/ml in 20% DMSO) at the same volume and the mixture was incubated at 4 °C for 24 h. After the reaction, the NPs or F-NPs were isolated by centrifugation, washed with PBS, and resuspended at 20 mg/ml in PBS. The amount of DEX adsorbed into the NPs was evaluated by a DEX ELISA kit (Neogen, Lexington, KY). The loading content and entrapment efficiency of DEX into the NPs were evaluated in the same manner as was used for the TR-OVA-NPs. DEX-NPs or DEX-F-NPs loaded at 50 μg per milligram NPs were prepared. The entrapment efficiency of DEX into the NPs was calculated using the following formula: (amount of adsorbed DEX / initial feeding amount of DEX) × 100. The DEX entrapment efficiency was approximately 25%.

2.6. Characterization of the NPs

The size of the γ-PGA-Phe NPs in the aqueous solution was measured by a dynamic light scattering (DLS) method using a

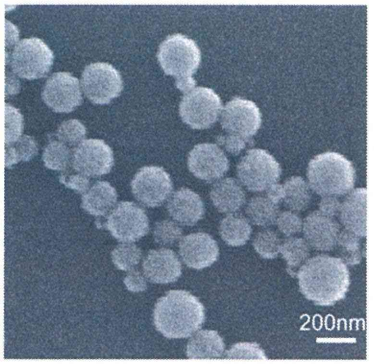

Fig. 1. SEM image of γ-PGA-Phe nanoparticles (NPs). Scale bar = 200 nm.

Zetasizer Nano ZS (Malvern Instruments, UK). The surface charge of the NPs was determined by zeta potential measurements using a Zetasizer Nano ZS. The NP suspension, diluted with PBS (100 μg/ml), was used without filtering to measure both particle size and zeta potential. The mean diameters of NPs, TR-OVA-NPs and DEX-NPs were 175 ± 33, 220 ± 65 and 180 ± 45 nm (mean ± SD), respectively. The zeta potential of the NPs was approximately −25 mV.

(Further information regarding the materials and methods used in this study is contained in "Supplementary data.")

3. Results

3.1. γ-PGA-Phe NPs are taken up by macrophages and microglia in vitro

Macrophages and microglia have been demonstrated to be involved in several pathological conditions of the retina including excitotoxicity [26], retinal detachment [22], and glaucoma [25]. Thus, we first investigated whether NPs can be taken up by those phagocytic cells *in vitro*. In cell culture, 200 nm NPs (Fig. 1) containing TR-OVA were incubated for 2 h and NPs taken up by macrophages and microglia were examined after washing out free TR-OVA-NPs. The signal for TR-OVA (Fig. 2) was co-localized with the cellular markers for macrophages (CD11b) and microglia (CD68) under a fluorescent microscope with 98% of cultured macrophages or microglia containing TR-OVA-NPs (Fig. 2). Analysis using confocal microscopy showed that the TR-OVA-NP signal was detected in the cytoplasm as a high-intensity, granular signal and in macrophages and microglia as a low-intensity, diffuse signal (Fig. 3).

According to flow cytometry analysis (Fig. 4), the TR-OVA-NPs are taken up by macrophages/microglia in a dose-dependent manner, according to the FL2-H histogram. The mean FL2-H indicates that macrophages have a higher capacity for phagocytosis than microglial cells.

3.2. Persistence of NPs in vitro

In our previous study, γ-PGA-Phe NPs were found to be degraded by various enzymes, such as Pronase E and cathepsin B, with different

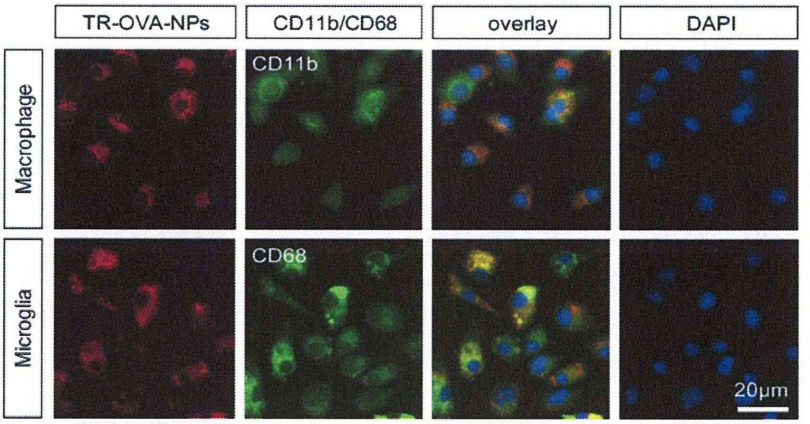

Fig. 2. Uptake of TR-OVA-NPs by cultured macrophages and microglia. The first lines indicate the signals from TR-OVA-NPs and the second lines indicate the immunoreactivity with CD11b, the cellular marker for macrophages (upper panel), and CD68, the marker for activated microglia (lower panel), in the cultured macrophages or microglia. Scale bar = 20 μm.

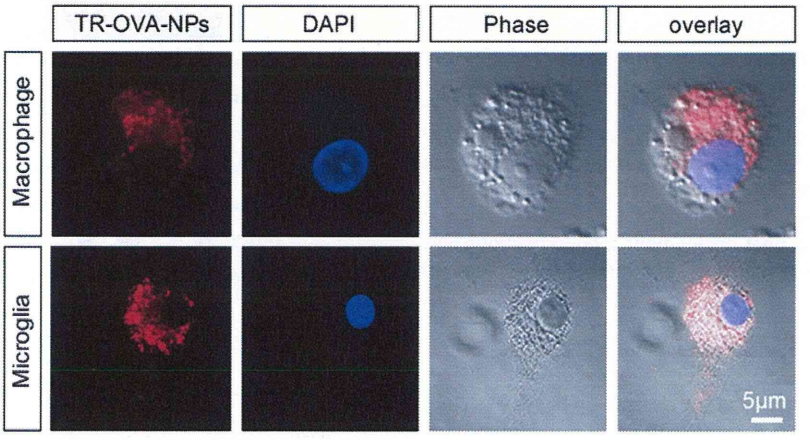

Fig. 3. Confocal images of the cultured macrophages and microglia with TR-OVA-NPs. TR-OVA-NP signaling was detected in the cytoplasm as a high-intensity granular signal and a low-intensity diffuse signal in the cultured macrophages and microglia. Scale bar = 5 μm.

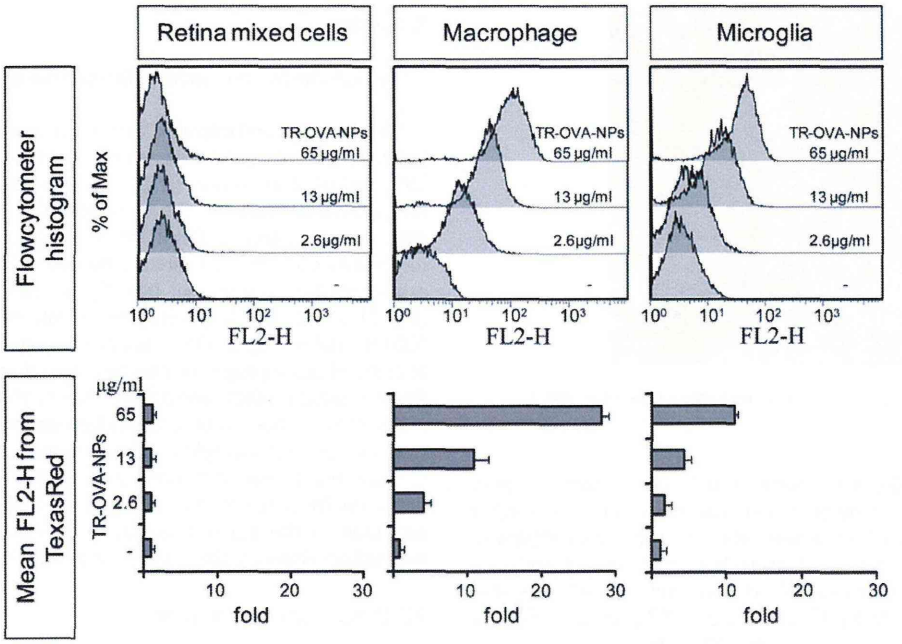

Fig. 4. Relative quantification of phagocytosed TR-OVA-NPs in retinal mixed cells, macrophages, and microglial cells. The histograms demonstrate that the TR-OVA-NPs are taken up by macrophages or microglial cells in a dose-dependent manner and that macrophages have a higher capacity to take up the NPs. TR-OVA-NP (13 μg/ml)-treated macrophages showed an approximately 12-fold increase in the mean FL2-H value compared to the control (0 μg/ml TR-OVA-NPs).

degradation patterns *in vitro*. The degradation and collapse of the NPs was attributed mainly to the cleavage of amide bonds between the α-carboxylate side chains of γ-PGA and Phe [14]. The degradation speed depends on the hydrophobicity (the grafting rate of the hydrophobic side chain) and the type of enzyme, suggesting that there are differences in degradation speeds between cell types. To investigate the degradation speeds and the persistence of TR-OVA-NPs in the cells of interest, the TR-OVA signals were quantified in macrophages and microglia at 2 and 7 days after the administration of NPs. Although the granular signal decreased to 20% on day 7, the diffuse signal remained around 80% in the cytosol of the cell (Fig. 5). According to this result, we presume that TR-OVA-NPs aggregated in cells should release a "granular signal" and the TR-OVA released from degraded NPs that remained in the cytosol should release a "diffuse signal" through the Cy3 filter in the fluorescein microscope. These data may suggest that 80% of the NPs in the macrophages/microglia get degraded on day 7 but that the contents released from the NPs persist in the cytosol.

3.3. NPs in normal and pathological conditions of the retina

To investigate drug dynamics *in vivo*, we injected TR-OVA-NPs into the vitreous cavity, harvested the eyes 2 days later, and prepared cryosections to investigate the distribution of NPs. When 0.8 or 4 μg of NPs were injected into normal, injury-free eyes, no NPs were taken up by the cells (Fig. 6). In the NMDA-damaged retina, resident microglia transformed from a dendritic shape to a spindle or amoeboid shape, reflecting the activated status of the microglia. NPs were taken up by these cells (Fig. 7). In the retinal detachment model, macrophages were recruited into the sub-retinal space and the NPs were taken up (Fig. 8).

3.4. DEX-NPs suppress inflammation both in vitro and in vivo

To be effective, drugs contained in the NPs should be released into the cytoplasm [14].

Thus, an agonist for nuclear receptors or an inhibitor of a signal transduction pathway would be a good target for treatment. Here, we chose DEX as a popular and potent corticosteroid for anti-inflammatory conditions that is already used in the clinic. To test the potential of DEX-NPs to suppress inflammation, we examined changes in the expression of TNFα and MCP-1, major cytokines and chemokines

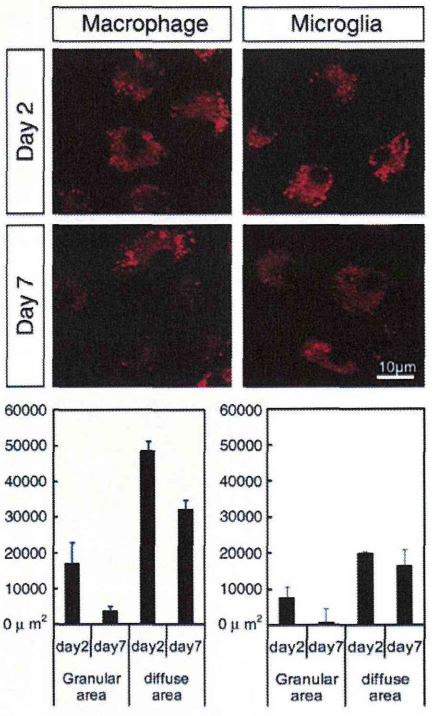

Fig. 5. Time course for the alterations in the persistence of TR-OVA-NPs. The photographs show the appearance of TR-OVA-NPs on day 2 (upper panels) and day 7 (lower panels) *in vitro*. The bar charts show the quantitative data for the area of granular, high-intensity, dot or diffuse cytoplasmic signaling in the cultured macrophages and microglia. Scale bar = 10 μm.

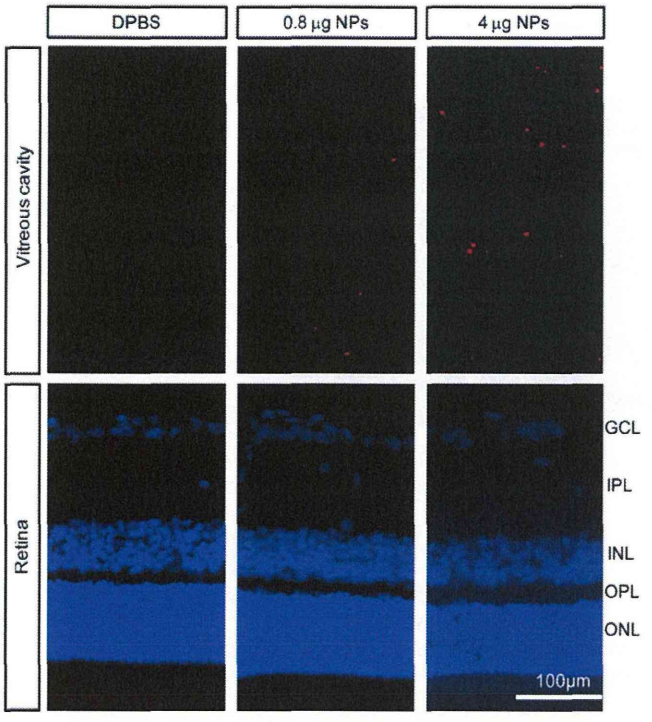

Fig. 6. Absence of accumulation of TR-OVA-NPs in the healthy retina. There was no accumulation of TR-OVA-NPs in the retina (lower panels). Some weak signals were detected in the vitreous cavity but not in any cells. Scale bar = 100 μm. GCL: ganglion cell layer, IPL: inner plexiform layer, INL: inner nuclear layer, OPL: outer plexiform layer, and ONL: outer nuclear layer.

released from cultured macrophages, with or without DEX-NPs (NPs 13 μg/ml, DEX 0.65 μg/ml). As a positive control, we used 0.65 and 6.5 μg/ml of DEX. At 3 and 24 h after application of the NPs, the expression of TNFα and MCP-1 was significantly decreased, with DEX-NPs and pure DEX having almost the same effect (Fig. 9). To investigate whether the released DEX still possessed an anti-inflammatory effect on cultured macrophages, we applied DEX (0.65 μg/ml) or DEX-NPs (13 μg/ml DEX-NPs, equivalent to DEX 0.65 μg/ml) for 2 h and then changed the culture medium to remove the extra compound. We then immediately stimulated the cells with TNFα (day 0) or further culture-treated the macrophages for 48 h (day 2) and then stimulated them with TNFα. After 3 h of TNFα stimulation, the TNFα mRNA was significantly increased both on days 0 and 2. Pretreatment with DEX alone significantly suppressed the TNFα-induced TNFα expression on day 0, but this effect disappeared 2 days after DEX treatment. In contrast, the accumulation of DEX-NPs in macrophages suppressed the TNFα-induced TNFα expression on both days 0 and 2 (Fig. 10). These data suggest that the anti-inflammatory effects of DEX-NPs last longer than that of DEX alone in cultured macrophages. According to our analysis of the degradation of NPs in macrophages (Fig. 5), we believe that the DEX-NPs in macrophages degraded from day 0 to day 7 and kept releasing DEX to suppress the expression of TNFα, although the amount of DEX-NPs in the macrophages and the amount of DEX released into the cytosol of the macrophages was not clear. We next investigated the effects of DEX-NPs when injected intravitreally in rat models of retinal diseases. In the model of NMDA-induced damage, the activation of microglia (ratio of amoeboid shape to resting shape, Fig. 11A) was significantly suppressed by treatment with DEX-NPs (Fig. 11B). At the same time, the DEX-NPs significantly reduced the loss of RGCs 7 days after NMDA treatment (Fig. 12)|.|In the RD model, DEX-NPs significantly decreased the number of TUNEL (+) photoreceptors in the outer nuclear layer 3 days after injury compared with NPs alone (Fig. 13).

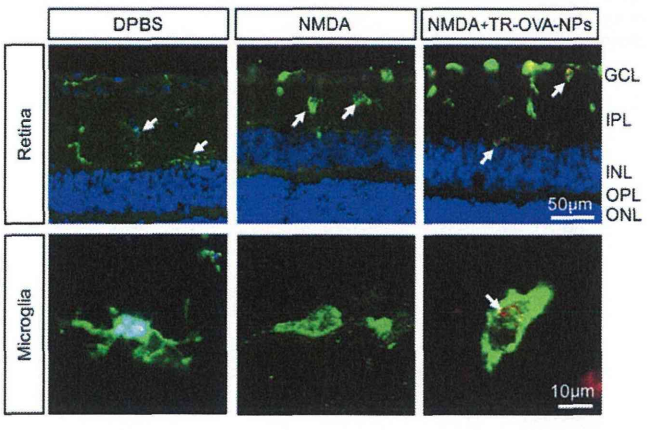

Fig. 7. Accumulation of TR-OVA-NPs in the active microglia in a model of NMDA-induced excitotoxicity. Without treatment with NMDA, microglia had dendrites that were observed to be in the resting phase (left-sided images). Treatment with NMDA induced the activation of microglia (amoeboid shape) in the IPL (center images). The activated microglia phagocytosed the TR-OVA-NPs in the damaged retina (right-sided images). Arrows indicate the microglia in the IPL. Scale bar = 50 μm (upper panels) and 10 μm (lower panels). GCL: ganglion cell layer, IPL: inner plexiform layer, INL: inner nuclear layer, OPL: outer plexiform layer, and ONL: outer nuclear layer.

4. Discussion

In this study, we first investigated the dynamics of γ-PGA-Phe NPs both *in vitro* and *in vivo*. In primary cultures of macrophages and microglia, TR-OVA-NPs were taken up by nearly all macrophages and microglia within which NPs were observed as bright puncta within the cytoplasm. These punctate signals gradually transformed into diffuse signals within the cytoplasm. On day 7, the cytoplasmic levels of TR-OVA were still visible in approximately 60 to 80% of the cells that showed staining on day 2. *In vivo*, the normal, undamaged retina showed no accumulation of NPs. Conversely, intravitreally administered TR-OVA-NPs accumulated in CD11b-positive, recruited macrophages and activated resident microglia in various pathological conditions including NMDA-induced retinal excitotoxicity and retinal detachment. Then, using DEX-NPs, we investigated whether a drug delivered by NPs worked effectively in the damage retina. DEX-NPs significantly suppressed the expression of TNFα and MCP-1 in cultured macrophages following TNFα stimulation. *In vivo*, intravitreal injections of DEX-NPs had a significant neuroprotective effect against NMDA-induced RGCs and RD-induced photoreceptor degeneration. These data suggest that γ-PGA-Phe NPs are a useful tool for the regulation of inflammatory phagocytic cells in the retina, especially under pathological conditions.

γ-PGA-Phe NPs persisted for more than 7 days in cultured macrophages. It has previously been reported that NPs become fragmented in dendritic cells and macrophages [14,28,30]. One purpose of using NPs as a delivery system was to provide more sustained drug release than that achieved when the drug is administered alone. We found that the TR-OVA-NPs were strongly detected at day 2 and that most signals were still present at day 7 in both the macrophages and microglia. Our results using cultured macrophages showed that DEX-NPs, but not soluble DEX alone, continued to suppress TNFα-induced upregulation of TNFα expression 2 days after a 2-h incubation with DEX-NPs followed by the removal of excess NPs from cultured macrophages. We previously demonstrated that macrophages and microglia were major players in the neurodestructive effects of RGCs and photoreceptors in various pathological conditions [22,25]. These data suggest that γ-PGA-NPs